Hydrogeology Journal
https://doi.org/10.1007/s10040-018-1890-3

PAPER

Impact of hotel septic effluent on the Jinfoshan Karst aquifer, SW China

Pingheng Yang [1,2,3] · Xiaoxing Ming [1] · Chris Groves [3] · Ting Sheng [1]

Received: 24 November 2017 / Accepted: 30 October 2018

Abstract

The karst aquifer of Jinfoshan Karst (JFK) in UNESCO's South China Karst World Heritage Site was investigated. An artificial tracer test, geochemistry, and oxygen and hydrogen isotopes were employed to assess the impacts of effluent from the Jinfoshan Holiday Hotel (JHH), Chongqing, on the karst aquifer and its outlet, Shuifang spring (SFS). Most of the fluorescent dye (uranine) flushed into a JHH toilet was recovered at SFS, suggesting a strong hydraulic connection between JHH and SFS. The waters of SFS were of HCO_3–Ca type, whereas the effluent had more complex hydrochemical characteristics. The effluent was characterized by higher mean δD and $\delta^{18}O$ values. The slope of the δD–$\delta^{18}O$ evaporation line for effluent was significantly lower than that of the local meteoric water line, indicating evaporation. Concentrations of major elements at SFS were below the threshold values of the Chinese Standard for Groundwater Quality. However, hydrogen and oxygen isotopic compositions of SFS waters were influenced by the effluent and mixing with water from diffuse sources within the aquifer. Low values of d-excess at SFS corresponded well to periods of high tourism activity (weekends and holidays), suggesting that declining d-excess probably signifies an increased release of contaminants from the hotel. The contribution of effluent to the discharge of the SFS was ~18%. Because of tourism activities and their production of wastewater, the results of this study may be relevant to other karst environments and World Heritage Sites throughout the world.

Keywords Karst · Septic effluent · Tracer test · Stable isotopes · China

Introduction

Onsite wastewater treatment systems, commonly known as septic systems, are the predominant method of wastewater treatment in rural areas without municipal sewage treatment alternatives. Most septic systems have two basic components: a septic tank and a drainfield (Toor et al. 2011). Simple in design, septic systems are normally recognized as a low-cost, long-term, decentralized and viable means of removing contaminants from household wastewater before discharging the wastewater into the environment (USEPA 2002; Toor et al. 2011). Therefore, septic systems are widely used throughout the world—for example, nearly 25% of households in the United States and 33% of households in Florida have septic systems (Toor et al. 2011), while in Australia, approximately 17% of the population relies on these systems to treat and dispose of wastewater (Carroll and Goonetilleke 2005).

Conventional septic tanks allow solids to settle and liquid effluent to flow out to a drainfield where the effluent percolates downward through the soil and unsaturated zone eventually reach the groundwater. Septic systems are sometimes located near shallow domestic wells or springs, which increases the probability of a direct connection between the septic system and the groundwater (Pei et al. 2003). In karst terrains, such situations present a particular risk for the rapid movement of bacteria, viruses, nitrogen, and other pollutants into groundwater because karst aquifers are known to be generally more vulnerable to contamination than those aquifers in nonkarst areas (Ford and Williams 2007; Goldscheider 2005; Katz et al. 2010). Eventually, the mobile constituents may discharge to the surface water (Iverson et al. 2015). Water contaminated by human effluent can cause a variety of waterborne diseases.

✉ Pingheng Yang
pinghengyang@126.com

[1] Chongqing Key Laboratory of Karst Environment, School of Geographical Sciences, Southwest University, No. 2 Tiansheng Road, BeiBei District, Chongqing 400715, People's Republic of China

[2] Key Laboratory of Shale Gas and Geoengineering, Institute of Geology and Geophysics, Chinese Academy Sciences, Beijing 100029, China

[3] Crawford Hydrology Laboratory, Department of Geography and Geology, Western Kentucky University, Bowling Green, KY 42101, USA

Published online: 10 November 2018

Karst aquifers are very vulnerable to various pollution sources (e.g. Jiang et al. 2008; Jiang et al. 2009). Many examples have proved that human activities such as agriculture and farming (e.g. Ekmekci 2005; Mellander et al. 2012), urbanization (e.g. Amiel et al. 2010; Bodhankar and Chatterjee 1994), landfills (e.g. Kogovšek and Petrič 2013; Ghobadi et al. 2017), and mining (e.g. Gong et al. 2014) can result in pollution that often influence karst groundwater quality and can contaminate drinking water.

In recent decades, high-resolution artificial tracer tests have been used to investigate the hydraulic connection within karst aquifers (e.g. Goldscheider et al. 2003; Goldscheider 2008; Lauber and Goldscheider 2014). With these methods, artificial tracers are injected into the karst aquifer to label flowing water, constituting useful tools to better understand the karst aquifer networks. They are also used to prove a hydraulic connection between a sinkhole and a spring and more broadly to delimit the boundary of the catchment area of a spring (Goldscheider et al. 2008).

Major elements (e.g. Yang et al. 2010), nitrate isotope (e.g. Jiang et al. 2009), phosphorus (e.g. Mellander et al. 2012), pesticides (e.g. Ekmekci 2005), bacteria (e.g. Pronk et al. 2007), and even pharmaceutical compounds, personal care products, and hormones (e.g. Dodgen et al. 2017) have been used as indicators/tracers for karst groundwater pollution. Selected physicochemical parameters of karst groundwater have become one of the most important methods to study hydrogeochemistry and the factors influencing karst groundwater (e.g. Mahler and Massei 2007; Yang et al. 2013). The isotopes ^{2}H and ^{18}O are natural components of water. Despite their typically low concentrations, ^{2}H and ^{18}O have sensitive responses to the regional environment and can record the process of water circulation (Craig 1961; Zang et al. 2015). Through analysis of the deuterium excess (d-excess = $\delta D - 8\delta^{18}O$; Dansgaard 1964), one can determine the degree of evaporation of a water body and identify the source of air mass. Using different geochemical and isotopic characteristics of various waters, studies have successfully traced the impact of wastewater discharge on groundwater resources (e.g. Rapti-Caputo and Martinelli 2009; Schiavo et al. 2009; Vanderzalm et al. 2011) and calculated the ratio of different recharge sources (e.g. Duque et al. 2011; Grimmeisen et al. 2017).

Recently, tourism has become an important type of recreation that stimulates local economic growth (Yang et al. 2009). Wastewater discharges due to tourism activities can cause substantial negative impacts on vulnerable karst groundwater systems, but documented reports are rare (Milenic et al. 2014). Jinfoshan Karst (JFK), located in Chongqing, southwestern China, was included in the World Heritage List in 2014 as part of the South China Karst Phase II (UNESCO 2014a). It is also a popular tourist destination, and was ranked nationally as a 5A scenic spot in 2013, the highest ranking by China's Ministry of Culture and Tourism for the most important and best maintained sites. Every year, a large number of tourists visit JFK, especially during holidays and festival periods. This results in a substantial increase in domestic water demand and generates a large amount of hotel wastewater that is treated by a septic system and then drains into the karst aquifer.

It is hypothesized here that the septic effluent of hotel, which are point source, affects the hydrogeochemistry and water quality of the karst aquifer. The objective of this study therefore is to obtain insight into the impacts of septic effluent on the underlying karst aquifer, focusing on the following goals: (1) to investigate the hydraulic connection between the pollution source and the aquifer's principal spring outlet with an artificial tracer test; (2) to evaluate the geochemical and stable hydrogen and oxygen isotopic characteristics of the effluent and the karst groundwater; (3) to quantitatively assess the contribution of the effluent to karst groundwater based on the stable isotopes of hydrogen and oxygen. On a broader scale, this study illustrates the characteristics of karst environments impacted by the wastewater throughout the world, because of the widespread global tourism activities and their production of wastewater, including groundwater within numerous karst-rich World Heritage Sites.

Materials and methods

Study area

Location and geographical setting

The JFK is located in Nanchuan District of Chongqing, China, with a summit elevation at Fengchui Peak of 2,251 m above sea level (asl; Fig. 1). It lies in the landscape transition zone between the southeastern margin of the Sichuan Basin and the Yunnan–Guizhou Plateau on the north slope of Daloushan Mountain. This region of southwestern China has a subtropical humid monsoon climate; however, the study area is located at an elevation of >2,000 m on the upper part of the mountain and is therefore subject to a local temperate climate, with an average annual temperature of 8.2 °C and precipitation of 1,434 mm/year, respectively. The rainfall is mainly concentrated in the period from April to October.

Hydrogeological setting

The aquifer is developed within Permian carbonate rocks, with flow dominated by an underground river system which discharges via a karst spring. A series of karst landforms, including depressions and sinkholes, are developed in the carbonate rocks formed on the mountain tableland surface. The karst hydrogeological conditions of the watershed are characterized by an approximately 20-m-thick unsaturated zone, a heterogeneous and anisotropic interior structure, and highly

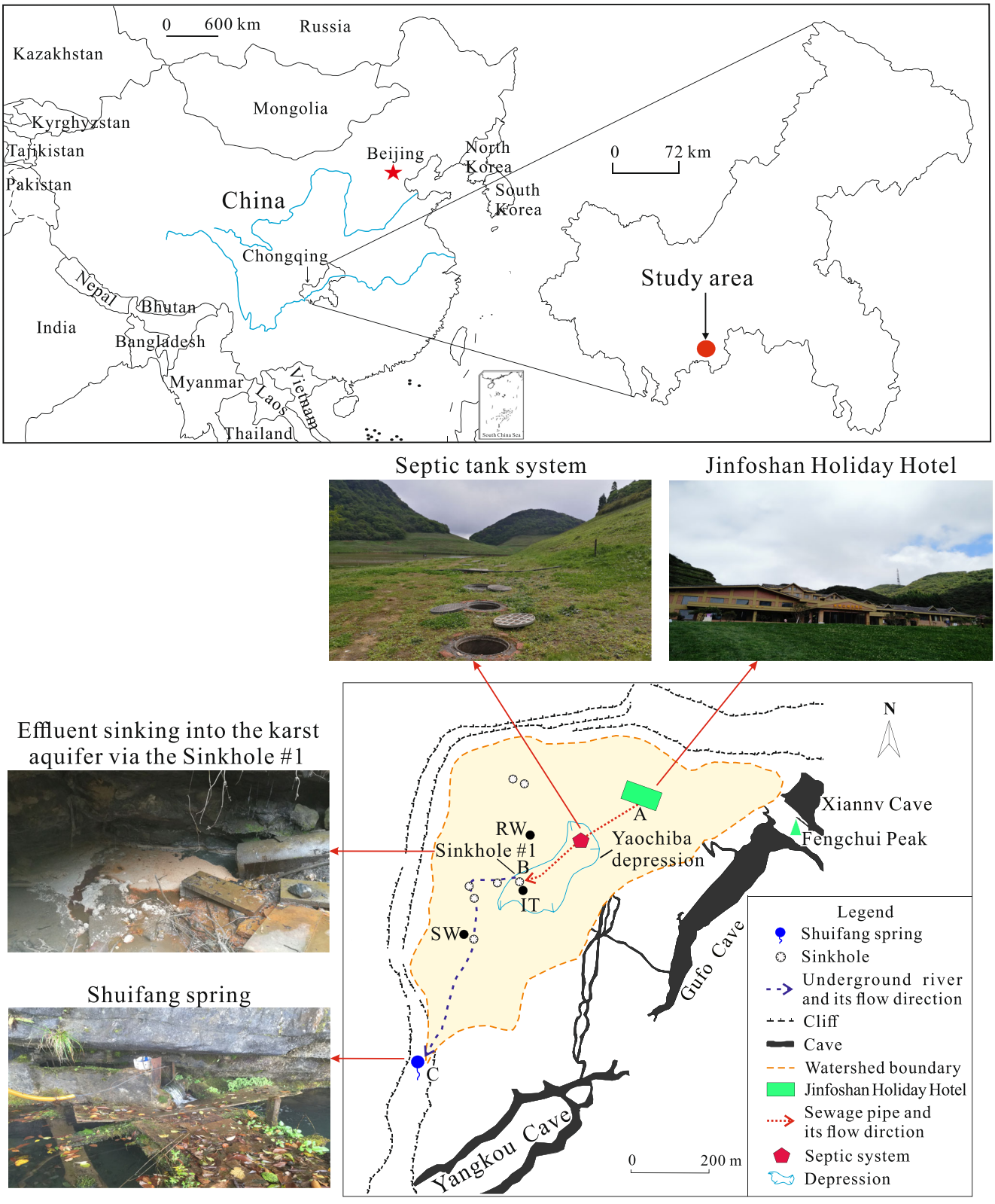

Fig. 1 Location of the study area, and a hydrogeological schematic map (modified from Wu et al. 2008). RW rainwater collection site. SW soil water collection site. IT injection site of an irrigation tracer test (Lettingue 2007)

variable input and output (Wu et al. 2008). The heterogeneity and anisotropy of the system's structure results from the extreme range of hydraulic conductivities among the epikarst zone, large conduits and diffuse flow regions within a matrix dominated by microfractures beneath the surface (Fig. 2). The shallow carbonate aquifer at a depth of 30–120 m is separated

by a horizon of coal with ~10 m thickness that overlies a deeper carbonate confined aquifer. In most parts of the region, the karstified rocks are covered by yellow–brown loamy soils with average thickness of 0.8–1.2 m, but quite unevenly distributed with a maximum depth to 18 m (Wu et al. 2008), particularly in the depressions. The study area is overgrown by vegetation. As is common in well-developed karst flow systems, surface water is not present in this area since precipitation sinks quickly into the aquifer to reach the underground river conduit system (Figs. 1 and 2). The main entrance of the underground river is sinkhole No. 1, which lies at an elevation of ~2,090 m asl at the margin of the Yaochiba depression. Its outlet is Shuifang spring (SFS), which lies at an elevation of 2,053 m asl. The lateral distance between sinkhole No. 1 and SFS is ~526 m. The water of SFS is drained into a pool and then pours along the cliff forming a stream. The underground river network comprises a hydrological system with a recharge area of approximately 1.5 km^2. The SFS, a perennial karst spring, has a highly variable discharge from 0.5 to 38 L/s with an average of 6.5 L/s (Jiang et al. 2013). The aquifer drained by SFS is rapidly recharged through conduits and slowly recharged by low inflow from the fissured aquifer matrix (Wu et al. 2008).

Based on geological surveys, the carbonate basin of the JFK formerly had a large drainage area with abundant precipitation and a large and well–developed karst underground river system. Neotectonic uplift, river capture, and headward erosion destroyed the original drainage basin, and only a smaller tableland surface at an elevation of approximately 2,100 m asl remains, which is surrounded by steep cliffs. The former underground rivers have evolved into dry caves with very large passages such as Gufo Cave, Yangkou Cave, and Xiannv Cave in the eastern and southern part of the study area (Fig. 1). The JFK records the process of dissection of the high-elevation karst plateau and contains evidence of the region's intermittent uplift and karstification since the Cenozoic Period. It is a superlative type-site of a karst table mountain (UNESCO 2014b).

Human activities and potential pollution

The JFK is an important tourist destination for Southwest China and attracts a large number of tourists every year. Since 2000, the Ice and Snow Festival (from mid-December to mid-February) and the Azalea Festival in early May have been held every year. According to one estimate, 519,100 people visited JFK in 2014. The Jinfoshan Holiday Hotel (JHH), with a total of 96 suites, 195 beds and a dining hall for 620 people, is located near the upper stream of the SFS basin which is in the core zone of the JFK. The domestic wastewater derived from the JHH is treated by a buried septic system (Fig. 1). The septic tank effluent, acting as a point source, sinks directly into the karst aquifer at sinkhole No. 1 through a sewage pipe. In a 2007 site reconnaissance (Lettingue 2007), bacteriological contamination was measured at SFS with 158 thermotolerant coliforms per 100. This concentration was induced by a high runoff event, forwarding the wastewater by the tourist village directly into sinkhole No. 1 without soil filtration. This suggests that the microbial contamination caused by tourist activities was quite serious at that time.

Research methods

Artificial tracer test

The aim of this artificial tracer test experiment was to determine if a hydraulic connection exists between the sinkhole No. 1 and SFS. The fluorescent dye uranine (sodium fluorescein) was used as a conservative tracer (e.g. Geyer et al. 2007). The dye (517.8 g) was flushed into a toilet in a room within the JHH at 20:10 on January 17, 2015. The tracer test was finished at 13:00 on February 2, 2015. Before injection, a field spectrofluorometer GGUN-FL30 with an excitation of 470 nm and a measurement limit of 0.01 μg/L (Albillia Sarl, Switzerland; Schnegg and Costa 2002) was installed at SFS to monitor the concentration of uranine. Its measurement interval was set at

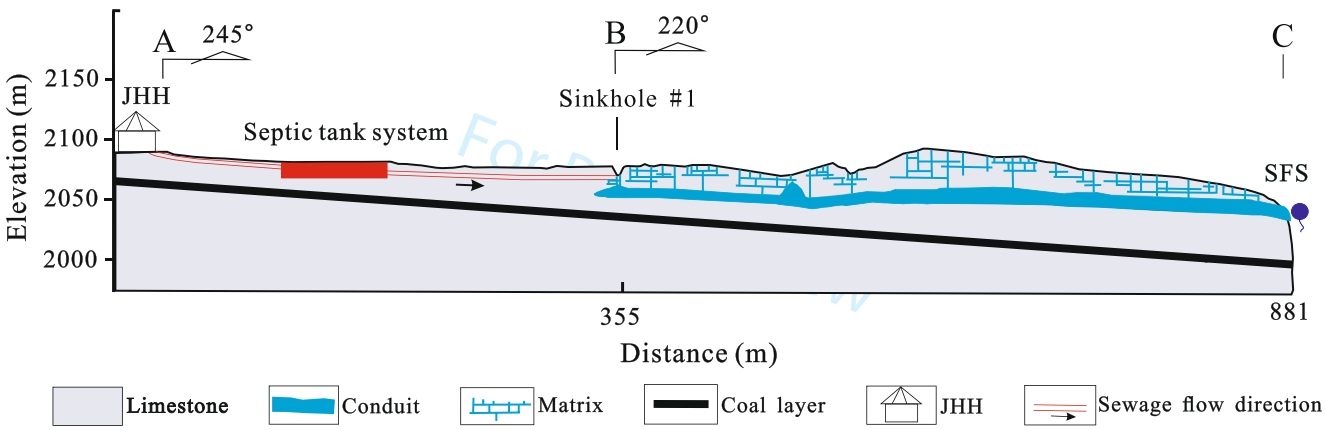

Fig. 2 A hydrogeological cross-section of the study area

10 min. The mass recovery is calculated by multiplying discharge by the concentrations of uranine. The discharge was converted from the water stage using a rating curve, which is expressed as the following empirical formula: $Q = 1.86\ Bh^{2/3}$ (Wang 2011), where Q is the discharge (m^3/s), B is the weir width of SFS with a value of 0.3 m, and h is the water stage of SFS (m). The water stage was automatically recorded using a Manta2 multi–parameter analyzer (Eureka, USA), with an accuracy of 0.01 mm. The lateral distance from the JHH to sinkhole No. 1 is ~335 m, and it is 526 m from sinkhole No. 1 to SFS, so the total lateral distances from the JHH to SFS is ~881 m (Fig. 2).

Field sampling and monitoring

Local meteoric water samples were collected following standards of the International Atomic Energy Agency's Global Network of Isotopes in Precipitation (IAEAGNIP). Of these, 18 samples were subjected to stable hydrogen and oxygen isotope analysis, and eight of them were also tested for physicochemical data. Soil water samples were collected from 20 and 60 cm depths in a depression (Fig. 1), and nine samples were taken at each depth for stable hydrogen and oxygen isotope analysis. Samples were taken between January 4, 2015 and April 3, 2016. Additional data can be found in Chen and Li (2018).

A total of 17 effluent samples were manually collected from the septic tank outlet at sinkhole No. 1 for stable hydrogen and oxygen isotope analysis between January 4, 2015 and April 3, 2016, and 12 of those samples were also used for measuring physicochemical parameters in situ.

Water samples (1 L) at the SFS were collected using a Sigma 900 autosampler (Hatch, USA) at 1-day intervals from September 24, 2014 to May 7, 2015, and from October 21, 2015 to April 3, 2016. The samples were used to analyze cations, ions, and stable hydrogen and oxygen isotopes. The sampling was partially interrupted due to equipment failure, and a total of 210 samples were collected to measure the oxygen and hydrogen isotopes and major elements. Of these, 12 samples of water temperature (WT), pH, specific conductance (SpC), and dissolved oxygen (DO) were measured in situ. To prevent degassing and water vapor exchange in the water samples, ~20 ml of liquid paraffin was added into sample bottles before sampling. In addition, NH_4^+ concentrations were measured in nine samples of effluent and from SFS from March 12, 2016 to August 18, 2016.

The water samples were stored in 10-ml-brown-glass bottles for stable hydrogen and oxygen isotope analysis or in 50 and 800-ml-polyethylene bottles for cation and anion analysis, respectively. All water samples were filtered through a 0.45-μm-membrane filter. A few drops of 1:1 HNO_3 were added into the samples used for cation analysis to adjust the pH to <2 and maintain the ionic activity. After pretreatment, the samples were transported to the laboratory and stored at 4 °C.

Analytical techniques

WT, pH, SpC, and DO of the effluent and SFS samples were measured in the field using a WTW 3430 multiparameter meter (WTW, Germany); the accuracies of the parameter measurements were 0.1 °C, 0.001 pH unit, 1 μS/cm, and 0.01 mg/L, respectively. All instrument probes were calibrated before use in the field. Cations were measured using an Optima 2100DV ICP–OES (PerkinElmer, USA), and the relative standard deviation of the equipment within 1 h was ≤0.5%. Anion measurements were conducted in accordance with the Chinese standard of GB/T 8538–2008 (State Bureau of Technical Supervision of China 2008). HCO_3^- concentrations were measured by titration using a field alkalinity test kit (Merck, Germany) with an accuracy of 0.1 mmol/L. For all samples, the concentrations of cations and anions were subjected to a charge balance check at ≤±5%. The NH_4^+ concentrations were determined in situ immediately after collection using a DR2800 spectrophotometer (Hach, USA), which had accuracies of 0.01 mg/L.

$\delta^{18}O$ and δD were measured using an IWA-35d-EP liquid water stable isotope analyzer (LGR, USA). The absolute errors of the $\delta^{18}O$ and δD analyses were less than 0.1 and 0.3‰, respectively. The ratio of stable isotopes ($^{18}O/^{16}O$ or $^{2}H/^{1}H$) was reported in parts per thousand (‰) relative to the Vienna Standard Mean Ocean Water (V-SMOW). The aforementioned sample analyses were carried out in a geochemistry and isotope laboratory in the School of Geographical Sciences, Southwest University, China.

Results and discussion

Artificial tracer test

The artificial tracer test parameters are summarized in Table 1. Most (82.5%) of the injected tracer was recovered, indicating that SFS is the main drainage outlet of the water release from the JHH, at least the wastewater from the flush toilets. The breakthrough curve (BTC) shows a plateau-like shape with two secondary concentration peaks (Fig. 3). The plateau-like phase lasted from 44.8 to 90.3 h after injection with similar concentrations of tracer near 123 μg/L. A plateau-like BTC following instantaneous injection is expected where there is an intermediate storage of tracer in large cavities that contain quasi-immobile groundwater and a slow release into active conduits (Goldscheider et al. 2003). This plateau-like shape of the studied case thus may be attributed to the intermediate storage of the tracer in the septic tank system and its gradual release into the aquifer via

Table 1 Summary of artificial tracer test

Tracer	*M* (g)	*D* (m)	tf (h)	mv (m/h)	tm (h)	dv (m/h)	*R* (%)
Uranine	517.8	881	26.8	32.9	67.6	13	82.5

M mass of injected tracer; *D* lateral distance between JHH and SFS; *tf* time of the first detection of the tracer; *mv* maximum velocity; *tm* time of detection of the maximum concentration; *dv* dominant apparent flow velocity; *R* tracer mass recovery

sinkhole No. 1. As the curve shows no clear concentration peak among the plateau-like section, the time of the maximum concentration (tm) was arbitrarily selected from the middle point of the plateau-like curve, i.e., 67.6 h after the injection. The time that the tracer was first detected (tf) was 26.8 h after the injection. A maximum flow velocity (mv) and a dominant apparent flow velocity (dv) therefore are calculated as 32.9 and 13 m/h, respectively.

In addition, there were two secondary peaks in the BTC after 109.4 and 201.6 h after the injection (Fig. 3). Field and Leij (2012) simulated the BTCs and showed that multiple peaks on a BTC can be caused by pools or auxiliary conduits (bifurcated flow paths) in a karst aquifer. The dual secondary peaks are therefore probably attributable to the main conduit and a pool or a bifurcated flow path in the main conduit between sinkhole No. 1 and SFS. This is confirmed by injection of uranine and tinopal CBS-X dye as tracers into the sinkhole No. 1 and a double-peaked recovery curve for uranine and tinopal CBS-X recording at the SFS (unpublished data). The difference between the tf value and the time when it decays to the natural background level (tn) can be used to indicate the time required for polluted groundwater to revert to a natural background (Magal et al. 2013). Due to technical difficulties, the tracer tests were stopped before the tracer concentrations had reverted to background levels (Fig. 3). Exponential function fitting of the BTCs was therefore carried out to obtain an estimated tn value, which was 56.2 days. This result indicates

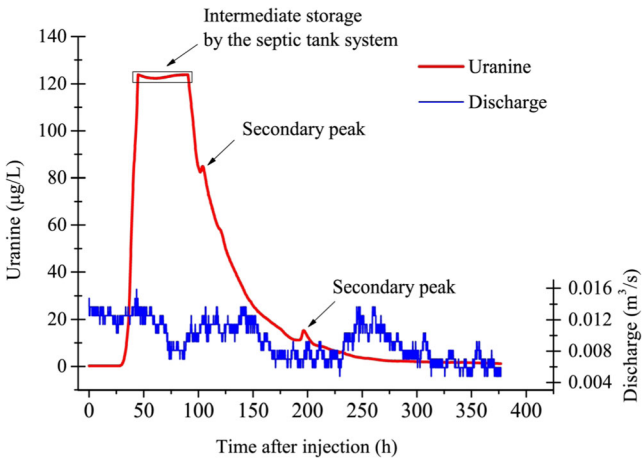

Fig. 3 Breakthrough curve of the artificial tracer test from a flushed toilet of the JHH

that a short-term pollution event produced at the JHH could have long-term (approximately two months) impacts on the quality of SFS, regardless of biodegradation, absorption or reaction with other substances in the groundwater. Lettingue (2007) carried out an irrigation tracer test using uranine as the tracer in a location inside the catchment area of SFS (Fig. 1). However, the tracer did not arrive at the spring for 2 weeks, which means that the soil and the epikarst constitute a mechanism to partially ameliorate contamination at SFS. Consequently, the main risk of contamination for SFS is induced by the effluent which recharged into the aquifer and transported in the conduit system.

Hydrogeochemical characteristics

A statistical summary of major element concentrations of rainwater, effluent and SFS is presented in Table 2. In the rainwater, pH ranged from 4.41 to 6.22, with a mean of 5.24 ± 0.74, which indicates that acid rain could occur in the study area previously thought to be pristine due to regional deposition of air pollution (Larssen et al. 2006). SO_4^{2-} and Ca^{2+} were the major ions, whose concentrations ranged from 3.03 to 14.8 and 1.30 to 5.89 mg/L, respectively, with means of 6.52 ± 4.06 and 2.57 ± 1.59 mg/L, respectively. SO_4^{2-} constituted 36.9–80.8% of the total equivalent of anions, which is in agreement with the fact that sulfate is the dominant anion in precipitation in China (Tang et al. 2001). Ca^{2+} constituted 31.5–85.1% of the total equivalent of cations, which is consistent with regional air pollution in China characterized by the high concentration of base cations in the atmosphere (Larssen and Carmichael 2000). Additionally, Cl^- concentrations ranged between 0.71 and 3.55 mg/L, with a mean of 1.78 ± 1.03 mg/L and accounting for 13.5–42.6% of the total equivalent of anions. The concentrations of K^+, Na^+, Mg^{2+}, and NO_3^- were relatively low, with means of 0.44 ± 0.11, 0.61 ± 0.68, 0.26 ± 0.35, and 0.94 ± 0.72 mg/L, respectively. Overall, the hydrochemical facies of rainwater were complex, including SO_4–Ca, SO_4 · Cl–Ca, SO_4 · Cl–Ca·Na, and SO_4 · Cl–Ca·Mg types (Fig. 4).

In the effluent, the WT ranged between 0.6 and 13.4 °C, with a mean of 7.09 ± 4.08 °C, while the pH was in the range of 6.45–7.77, with a mean of 7.36 ± 0.37. The SpC was within the range of 75.9–957 μS/cm, with a mean of 418 ± 283 μS/cm and the DO occurred in the range of 3.6–10.9 mg/L, with a mean of 7.20 ± 2.61 mg/L. The HCO_3^- and Ca^{2+} concentrations ranged from 79.3 to 281 and 35.2 to 58.1 mg/L, respectively, with means of 137 ± 52.2 and 44.5 ± 7.83 mg/L, respectively, accounting for 52.9–76.3% and 45.9–81.0% of the total equivalent of anions and cations, respectively. Na^+, Cl^-, and SO_4^{2-} were 18.8 ± 15.1, 21.5 ± 9.26, and 20.5 ± 11.0 mg/L, respectively. The NO_3^- concentrations were relatively low, with a mean of 5.53 ± 3.28 mg/L, whereas the NH_4^+ concentrations ranged from 1.23 to

Table 2 Statistical description of major element concentrations in rainwater, septic tank effluent, and SFS

Parameter	Rainwater				Effluent				SFS			
	Min	Max	Mean	SD	Min	Max	Mean	SD	Min	Max	Mean	SD
WT	4.4	15.3	11	6.58	0.6	13.4	7.09	4.08	9.37	10.2	9.85	0.17
pH	4.41	6.22	5.24	0.74	6.45	7.77	7.36	0.37	7.41	8.64	8.27	0.3
SpC	21.3	62.9	40.3	15.8	75.9	957	418	283	219	301	252	15.9
DO	6.78	11.2	9.1	1.4	3.6	10.9	7.2	2.61	5.37	8.8	7.99	0.43
K^+	0.28	0.57	0.44	0.11	1.63	22.3	8.02	6.5	0.35	2.14	0.81	0.43
Na^+	0.11	2.03	0.61	0.68	6.01	61.6	18.8	15.1	1.04	6.39	2.41	1.31
Ca^{2+}	1.3	5.89	2.57	1.59	35.2	58.1	44.5	7.83	42.8	58.5	50.8	2.39
Mg^{2+}	0.02	1.12	0.26	0.35	1.04	3.07	1.73	0.58	0.83	3.09	1.55	0.39
Cl^-	0.71	3.55	1.78	1.03	6.38	41.1	21.5	9.26	1.42	26.9	10.3	4.27
SO_4^{2-}	3.03	14.8	6.52	4.06	7.73	40.2	20.5	11	4.59	20.6	9.35	3.23
HCO_3^-	0	0	0	0	79.3	281	137	52.2	116	171	141	10.2
NO_3^-	0.05	2.39	0.94	0.72	1.9	12.3	5.53	3.28	2.72	24.3	8.59	3.83
NH_4^+	ND	ND	ND	ND	1.23	17.2	7.3	6.06	0.07	2.37	0.65	0.85

Ion concentrations (mg/L), WT (°C), SpC (20 °C in μS/cm), and DO (mg/L). *SD* standard deviation; *ND* not detected

17.2 mg/L, with a mean value of 7.3 ± 6.06 mg/L. After ammonification or mineralization in a septic tank, the nitrogen in the septic effluent is often largely in the form of NH_4^+ (Zhu et al. 2016), which makes the effluent rich in NH_4^+ and relatively poor in NO_3^-. With mixing of oxic groundwater, the high NH_4^+ has the potential to increase the NO_3^- concentration via nitrification (Umezawa et al. 2009). The effluent showed complex hydrochemical facies, including HCO_3–Ca, HCO_3 · Cl–Ca, HCO_3–Ca · Na, HCO_3 · Cl–Ca·Na, and HCO_3 · Cl · SO_4–Ca (Fig. 4).

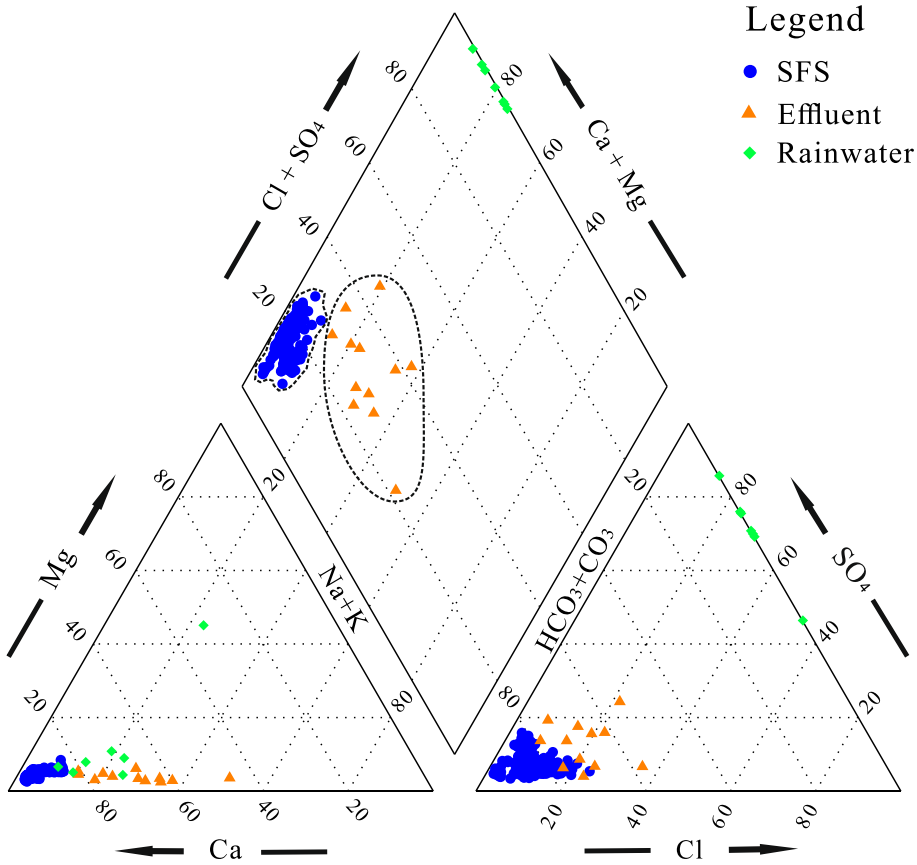

Fig. 4 Piper diagram showing the distribution of the chemical compositions of rainwater, SFS and septic tank effluent. The effluent samples show complex geochemical facies, while the SFS samples belong to HCO_3–Ca geochemical facies

At the SFS, the WT ranged between 9.37 and 10.2 °C, with a mean of 9.85 ± 0.17 °C, while the pH ranged from 7.41 to 8.64, with a mean of 8.27 ± 0.3, which was higher than that of the effluent and showed the weakly alkaline characteristics of the karst region. The SpC fell in the range of 219–301 μS/cm, with a mean of 252 ± 15.9 μS/cm. The DO was in the range of 5.37–8.8 mg/L, with a mean of 7.99 ± 0.43 mg/L, which was higher than that of the effluent. HCO_3^- and Ca^{2+} were dominant in the SFS water. The HCO_3^- concentrations fell in the range of 116–171 mg/L, with a mean of 141 ± 10.2 mg/L and accounting for 67.4–87.5% of the total equivalent of anions. The Ca^{2+} concentrations ranged between 42.8 and 58.5 mg/L, with a mean of 50.8 ± 2.39 mg/L and accounting for 83.4–94.6% of the total equivalent of cations. Compared with the effluent data, low levels of Cl^-, SO_4^{2-}, K^+, and Na^+ were present in the SFS, with means of 10.3 ± 4.27, 9.35 ± 3.23, 0.81 ± 0.43, and 2.41 ± 1.31 mg/L, respectively. The hydrochemical facies were of the HCO_3–Ca (Fig. 4), whereas the NO_3^- and NH_4^+ concentrations were 2.72–24.3 mg/L with a mean of 8.59 ± 3.83 mg/L, and 0.07–2.37 mg/L with a mean of 0.65 ± 0.85 mg/L, respectively. It should be noted that the mean NO_3^- was much higher than that of effluent, and the mean NH_4^+ concentration was much lower than that observed in the effluent (Table 1). This result is ascribed to nitrification occurring in the karst conduit, where NH_4^+ from the effluent was rapidly and completely converted to NO_3^- by nitrification and mixing of relatively oxygen-rich groundwater from the matrix (Umezawa et al. 2009; Grimmeisen et al. 2017).

The major element concentrations as indicated by SpC in the effluent were much higher than that observed at SFS (Table 1), demonstrating that the element concentrations of the effluent are higher than those of SFS. The hydrochemical facies of the effluent were also substantially different from those of the SFS (Fig. 4), reflecting different geochemical environments between the effluent and SFS. The SFS was rapidly recharged through conduits and slowly recharged by low inflow from the fissured aquifer matrix (Fig. 2; Wu et al. 2008). So the effluent that sank into the aquifer via sinkhole No. 1 was greatly diluted by the relatively unpolluted groundwater from the karst matrix, which rendered the geochemical type of SFS to be HCO_3–Ca, the most typical geochemical facies in karst environments (Ford and Williams 2007). According to the *Standard for groundwater quality* (General Administration of Quality Supervision, and Inspection and Quarantine of the People's Republic of China 2017), the related major element concentrations of the SFS belonged to class II which means that the water quality was suitable for various purposes.

Stable hydrogen and oxygen isotopes

In the rainwater samples, the δD and $\delta^{18}O$ ranged from −84.3 to −0.6‰ and − 12.0 to −3.1‰, respectively, similar to the range observed by Chen and Li (2018) from 2012 to 2016 outside of Yangkou Cave here at JFK, which has the same elevation and geological setting as the vicinity of the study area (Fig. 1). The δD and $\delta^{18}O$ values of rainwater show a wide distribution (Fig. 5a). These δD and $\delta^{18}O$ data produce a local meteoric water line (LMWL), i.e., $\delta D = 9.2\delta^{18}O + 28.3$ ($r^2 = 0.98$, $p < 0.01$). This LMWL has a steeper slope and higher intercept compared with the global meteoric water line (GMWL), $\delta D = 8\delta^{18}O + 10$ (Craig 1961). On the other hand, the slope and intercept of the LMWL are similar to those of the LMWL of $\delta D = 9.0\delta^{18}O + 24.6$ observed by Chen and Li (2018) from 2011 to 2016, and $\delta D = 8.8\delta^{18}O + 22.1$ observed by Wang et al. (2014) through the period of September 2011 to August 2013 outside of Yangkou Cave. Due to the different molecular masses of H and O, ^2H has a higher fractionation rate than ^{18}O under the same conditions; that is, the precipitation formed by multiple fractionation processes is enriched with ^2H, resulting in the steeper slope and higher intercept of the LMWL compared with the GMWL (Craig 1961). Therefore, the high slope and intercept of the LMWL suggests that precipitation in the study area was likely formed after several episodes of evaporation during transportation.

In the soil water at 20 and 60-cm depths, the ranges of δD values were −73.5 to −15‰ and −65.7 to −32.6‰, and the ranges of $\delta^{18}O$ values were −11.0 to −4.3‰ and −9.9 to −6.3‰. The δD–$\delta^{18}O$ evaporation lines were $\delta D = 9.4\delta^{18}O + 26.7$ ($r^2 = 0.99$, $p < 0.01$) and $\delta D = 9.5\delta^{18}O + 26.5$ ($r^2 = 0.99$, $p < 0.01$), which are almost parallel to the distribution of LMWL (Fig. 5). The δD–$\delta^{18}O$ evaporation lines have a slightly steeper slope than the LMWL, indicating almost negligible evaporation of soil water.

In the effluent, δD and $\delta^{18}O$ were in the ranges of −57.7 to −47.9‰ (mean − 52.7 ± 0.8‰) and − 8.9 to −5.4‰ (mean − 8.1 ± 2.9‰), respectively. The δD–$\delta^{18}O$ evaporation line of the effluent is denoted as $\delta D = 2.1\delta^{18}O + 35.8$ ($r^2 = 0.3$, $p < 0.01$). In the SFS, δD and $\delta^{18}O$ ranged from −62.1 to −51.1‰ (mean −54.8 ± 1.1‰) and −9.8 to −7.9‰ (mean −8.6 ± 0.2‰), respectively. The δD–$\delta^{18}O$ best-fit line of the SFS is denoted as $\delta D = 3.7\delta^{18}O + 23.0$ ($r^2 = 0.59$, $p < 0.01$). The effluent and SFS samples are distributed on the right side of the LMWL, and the slope of the fit lines are significantly lower than that of the LMWL (Fig. 5).

Karst groundwater is typically derived from the rainwater that infiltrates soil to enter the unsaturated zone and then penetrates into the saturated zone creating concentrated discharge in the karst conduits (Ford and Williams 2007; Yang et al. 2013). If the SFS was mainly recharged by rainwater, in theory, the stable hydrogen and oxygen isotopes of the SFS are distributed at both sides of the LMWL. However, the SFS

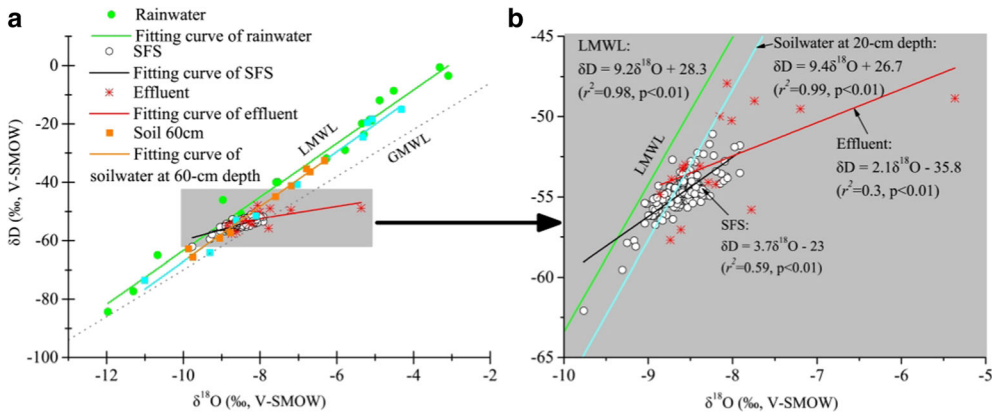

Fig. 5 **a–b** δD–δ^{18}O relationship. Septic tank effluent and SFS have much smaller slopes than the local meteoric water line (LMWL), indicating the effluent undergo isotopic enrichment

water actually has undergone significant isotopic enrichment compared with the local meteoric water (Fig. 5). The preceding analysis reveals that the rainwater has undergone little evaporation during soil infiltration; furthermore, the isotopes of drip water (representing water in the unsaturated zone) in Yangkou Cave are distributed on both sides of the LMWL, showing no significant evaporation (Wang et al. 2014; Chen and Li 2018). The means of δD and δ^{18}O in SFS (−54.8 and − 8.6‰, respectively) were much more positive than those in the drip water at Yangkou Cave (−57.1 and − 9.1‰, respectively; Wang et al. 2014) by 2.3 and 0.5‰, respectively. The SFS fit line intersects with the soil water evaporation line at −8.7 and − 55.3‰ (Fig. 5), which represents the initial isotopic composition of nonevaporated soil water recharging the SFS. Additionally, water–rock interaction has little effect on δD and δ^{18}O in groundwater at temperatures <90 °C (Mook 2000); therefore, the fractionation from soil to the unsaturated zone and water–rock interactions occurring in the aquifer have minimal impact on the enrichment of hydrogen and oxygen isotopes at SFS.

The slopes of the effluent and SFS fit lines were significantly lower than that of the LMWL (9.17), which indicates a stronger influence of kinetic versus equilibrium isotope effects (Gat 2010). Evaporation results in elevated δD and δ^{18}O values and in lower regression slopes (e.g. Grimmeisen et al. 2017); thus, the δD and ^{18}O samples distributed below the LMWL and with a lower slope than the LMWL suggest isotopic enrichment due to strong evaporation. Similar δD–δ^{18}O relationships with distinctively low slopes have been observed in polluted coastal groundwater (Schiavo et al. 2009), groundwater in an arid alluvial basin (Vanderzalm et al. 2011), and polluted karst groundwater in the city of As-Salt in Jordan (Grimmeisen et al. 2017). The effluent from the septic tank was mainly domestic sewage discharged from the restaurant and tourist facilities at JHH. Most of the wastewater, including water boiled or heated in kitchens and exposed to the air for a long time, or warm water from showers or laundry facilities, would obviously change ^{2}H and ^{18}O isotope signals, and results in the enrichment of hydrogen and oxygen isotopes and a less steep slope in the effluent at sinkhole No. 1. Thus, on one hand, the low slope and enrichment of hydrogen and oxygen isotopes of SFS water is ascribed to the drainage of the wastewater from the JHH into the aquifer via sinkhole No. 1 and mixing with diffuse groundwater. On the other hand, owing to the release of the wastewater into the karst aquifer, there were significant changes in the pH, SpC, DO, and turbidity of the effluent and the SFS concurrently. Specifically, the pH and DO are drastically decreased, whereas SpC and turbidity markedly are increased, and the overall water quality at SFS deteriorated during the peak tourist seasons (e.g. International Labor Day, Golden Week of the National Day in early October, the summer hot season in August, and the Ice and Snow Festival in the winter) on the basis of physicochemical data with a time step of 15-min in situ (unpublished data).

Compared with those of local meteoric water and soil samples, the δD and δ^{18}O values of the SFS water show a considerably narrow distribution (Fig. 5). The atmospheric signature in groundwater has undergone substantial changes, and the signature of stable hydrogen and oxygen isotopes in meteoric water is reduced via mixing of meteoric waters in the unsaturated zone (Guo et al. 2015; Pape et al. 2010). These generally make the isotope distribution more concentrated relative to that in local meteoric water, which means the SFS water does not show the seasonal signature from the rainfall, a finding which has also been observed in the groundwater of other places (e.g. Jin et al. 2012; Florea and McGee 2010; Schiavo et al. 2009). In the study area, the aquifer is highly sensitive to the external environment, and karst conduits are well developed; however, the overlying soil layer and the epikarst zone are relatively thick, resulting in a better developed rock matrix of diffuse flow that plays a significant role in regulation and storage of groundwater in the aquifer. Thus, the hydrogen and oxygen isotopes with a narrow distribution at SFS are a result of mixture of dominant diffuse flow and conduit flow in the study area, which does not reflect the seasonality, a finding which is also in agreement with the drip water observed by Chen and Li (2018), and Wang et al. (2014) in Yangkou Cave.

D-excess

Deuterium excess was defined by Dansgaard (1964) as d-excess = $\delta D - 8\delta^{18}O$, which is related to the meteorological conditions in the source region, e.g. relative humidity, temperature and wind. In the study area, the rainwater had d-excess in the range of 11.5–27.5‰, with a mean of 20.2 ± 4.8‰ that exceeds the mean d-excess of global meteoric water (10‰; Craig 1961). Owing to the altitude effect, water vapor in the air mass continuously falls in the form of rainwater when rising up a mountainside; consequently, d-excess increases with an increase in altitude (Gonfiantini et al. 2001). In the study area, the altitude is above 2000 m asl, and the elevation difference is more than 1,500 m higher than the lower part of the mountain, showing a significant altitude effect. Xiao (2015) has found that in the lower part of JFK at 719 m, the groundwater that was recharged by local meteoric water had a d-excess of only 8.3‰, which is significantly lower than the d-excess of rainwater in the study area. Thus, the altitude effect is responsible for the relatively high d-excess in rainwater in the study area. Water bodies subject to evaporative enrichment deviate from the GMWL and LMWL, signified by declining d-excess (Huang and Pang 2012; Turner et al. 2014). The d-excess consequently can be used to assess the effect of evaporation.

The d-excess parameter offers a possibility for characterizing the interaction of different air masses and their temporal evolution (Araguás-Araguás et al. 2000), and seems to be a good indicator of evaporative conditions (Benetti et al. 2014). An observational study by Huang and Pang (2012) has shown that in arid and semi–arid regions, the higher the evaporation rate of groundwater is, the higher the salinity, resulting in a negative correlation between d-excess and salinity (total dissolved solids) in groundwater. According to the previous discussion, the wastewater has undergone evaporation due to boiling in the kitchen, hot water used showers or washing, and exposure to the air in the JHH. The higher the SpC is, the lower the d-excess, resulting in a somewhat negative correlation between the two parameters to some extent (Fig. 6), which shows that the SFS is a mixture of the two end members. Therefore, if the wastewater has more evaporation, this means that the effluent had more impact on groundwater. It seems reasonable that one could use the d-excess as a proxy for the extent of contamination signifying the release of contaminants from the JHH. The d-excess of effluent ranged from −5.9 to 16.6‰, with a mean of 12.2 ± 5.5‰. The d-excess at SFS was between 9.8 and 17.0‰, with a mean of 14.1 ± 1.3‰, whereas the mean d-excess values of both the effluent and the SFS were lower than those of local meteoric water by 8 and 6.1‰, respectively, indicating that the stronger pollution occurred in the effluent than that in the SFS, which is consistent with the interpretations of this study.

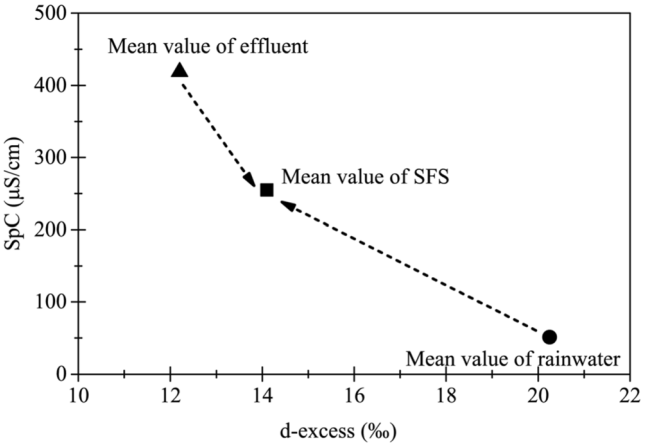

Fig. 6 A negative correlation between d-excess and conductivity. The arrows show that SFS is a mixture of the effluent and diffuse water within the aquifer, and suggest that decreasing d-excess probably signifies that water has deteriorated with increasing SpC

Weekends and holidays are the preferred time for travel and vacation. To further verify the impact of effluent on the d-excess of the SFS, the times of the low values of d-excess from the continuous SFS samples collected in the period of October 21, 2015 to April 3, 2016 were extracted in order to check whether they are consistent with the time of tourism activities. Statistical data show that the d-excess of the SFS had 17 low values below the mean (14.1‰), and 13 (76.5%) of them appeared on weekends or holidays (Fig. 7). In this period, the rainfall was 196 mm, and the water level showed a rapid response to rainfall. Even so, the preceding analysis has shown that the isotopic signature of rainwater in the SFS has been reduced, allowing for exclusion of the interference of d-excess by rainwater; therefore, the wastewater discharged by tourism activities had an important influence on SFS. Because the sampling interval of effluent data was relatively long, it was not possible to analyze the low values of d-excess in the effluent corresponding to the weekends and holidays; nevertheless, in the d-excess data of the effluent, the minimum of −6‰ appeared on the day before Christmas Eve, i.e., December 23, 2015 (Fig. 7). This was mainly due to the early arrival of numerous tourists for vacation (although Christmas is not a traditional holiday in China, it has become more popular with younger people in recent years). The corresponding d-excess of the SFS remained at low levels during December 23–24, 2015 (11 and 10.8‰, respectively), which further verifies the impact of wastewater from the JHH on the SFS.

The recharge rate of septic tank effluent to groundwater

The aforementioned analyses have demonstrated that the effluent and SFS had distinct characteristics of geochemistry and stable oxygen and deuterium. Thus, the effluent from the JHH can be treated as one single source of artificial

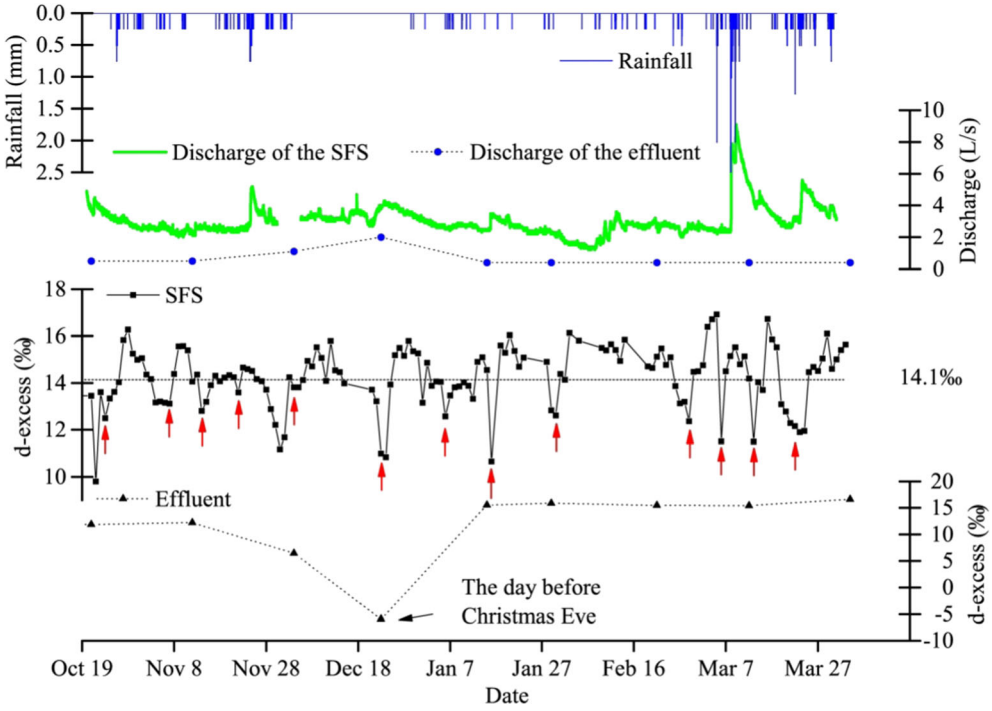

Fig. 7 Time series of d-excess in samples from SFS and septic effluent. Red arrows indicate the low values of d-excess on weekends and holidays. The results show good correspondence of low d-excess values to weekends and holidays, suggesting that the SFS is probably impacted by contaminant release from the tourism activities

recharge, and the recharge of effluents to the groundwater aquifer of the SFS basin can be quantified. In order to do so, a two-component mass balance of ^{18}O and ^{2}H was applied, an approach based on the mixing of two water bodies with markedly different signatures of stable hydrogen and oxygen isotopes, which has been extensively used in discharge separation studies (e.g. Laudon et al. 2002; Huth et al. 2004; Maurya et al. 2011; Klaus and McDonnell 2013). The two-component mass balance equation is:

$$\delta^{18}O_e x + \delta^{18}O_u(1-x) = \delta^{18}O_{SFS} \quad (1)$$

$$\delta D_e x + \delta D_u(1-x) = \delta D_{SFS} \quad (2)$$

where x is the proportional contribution of effluent to the SFS, $\delta^{18}O_e$ is the mean $\delta^{18}O$ of the effluent, $\delta^{18}O_u$ is the mean $\delta^{18}O$ of the unsaturated zone, $\delta^{18}O_{SFS}$ is the mean $\delta^{18}O$ of the SFS; δD_e is the mean δD of the effluent, δD_u is the mean δD of the unsaturated zone, and δD_{SFS} is the mean δD of the SFS.

$\delta^{18}O_e$ and δD_e are −8.1 and − 52.7‰, respectively, while $\delta^{18}O_u$ and δD_u are derived from the intersection of the SFS fitting line and soil water, i.e., −8.7 and − 55.3‰, respectively, and $\delta^{18}O_{SFS}$ and δD_{SFS} are −8.6 and − 54.8‰, respectively. The preceding $\delta^{18}O$ and δD are substituted into Eqs. (1) and (2) to calculate the contribution of effluent to SFS, that is, 16.7 and 19.2%, respectively, with a mean of 18%. As revealed by field observation, the discharge at sinkhole No. 1 was ~0.6 L/s (Fig. 7). The results of tracer tests have revealed that 82.5% of tracers injected at sinkhole No. 1 can be recovered from the SFS. The discharge of the SFS was found to be ~3 L/s on average over the study period. Accordingly, the contribution of effluent to the SFS is estimated to be 16.5%, which is consistent with the result obtained based on the two-component mass balance. The calculated contribution is similar to the fraction of wastewater of 0–20% spring discharge for individual large springs in the western margin of the Lower Jordan Valley (Schmidt et al. 2013).

Conclusions

Nutrient loading from septic tanks can have a serious impact on groundwater, especially in karst terrains due to the high vulnerability of these aquifers. The JFK is a popular tourist attraction and the groundwater quality has been threatened by wastewater derived from JHH. The combination of an artificial tracer test, geochemical analysis and stable hydrogen and oxygen isotopic composition is an effective tool to delineate the impact of septic effluent on the karst aquifer. There is a strong hydraulic connection between JHH and SFS. Although the major element concentrations of SFS are far below the threshold values for groundwater quality, and the effluent was greatly diluted by the groundwater from the karst aquifer matrix, the stable hydrogen and oxygen isotopic compositions were affected by the effluent. These slopes of best-fit lines of septic effluent and SFS are significantly lower than that of the LMWL, suggesting strong evaporation affecting the effluent, along with mixing of groundwater in the aquifer. The low values of d-excess of the SFS show good correspondence to weekends and holidays. Based on the two-component mass

balance, the effluent contributes 18% of the discharge to the SFS, resulting in a relative enrichment of stable hydrogen and oxygen isotopes in the SFS. Although these interpretations are consistent with our observations, there were a number of factors that were not taken into account—for example, quantitative consideration of air temperature and humidity, as well as the air mass source regions. In addition, the study did not fully consider the seasonal variations of the oxygen and hydrogen isotopes of the groundwater (e.g. Bar-Matthews et al. 1996; Carlson et al. 2018), and the effluent contribution on the spring discharge was at a comparatively low time resolution. However, the data firmly show that the karst aquifer of JFK is highly vulnerable to the impact of the effluent from tourism activities; therefore, managers need to develop reasonable policies and propose scientific protection measures. The ultimate goal of this paper is to provide background to enhance scientific protection for the vulnerable karst aquifers in China and throughout the world.

Acknowledgements The authors express gratitude to Guowen Xie, Zhengliang Yu, Feng Chen, Zhaojun Zhan, Juan Ren, Haiyue Zhang, and Zheyu Ma, for their help in the field sampling and laboratory work.

Funding information This work was supported by the National Key Technology R&D Program of China (2016YFC050230206, 2011BAC09B01), National Natural Science Foundation of China (41103068), and the Fundamental Research Funds for the Central Universities (XDJK2018AB002, SWU116087, and XDJK2017B13), and the China Scholarship Council.

Compliance with ethical standards

Conflict of interest The authors have no conflicts of interest to declare.

References

Amiel RB, Grodek T, Frumkin A (2010) Characterization of the hydrogeology of the sacred Gihon Spring, Jerusalem: a deteriorating urban karst spring. Hydrogeol J 18(6):1465–1479. https://doi.org/10.1007/s10040-010-0600-6

Araguás-Araguás L, Froehlich K, Rozanski K (2000) Deuterium and oxygen-18 isotope composition of precipitation and atmospheric moisture. Hydrol Process 14(8):1341–1355. https://doi.org/10.1002/1099-1085(20000615)14:8<1341::AID-HYP983>3.3.CO;2-Z

Bar-Matthews M, Ayalon A, Matthews A, Sass E, Halicz L (1996) Carbon and oxygen isotope study of the active water-carbonate system in a karstic Mediterranean cave: implications for paleoclimate research in semiarid regions. Geochim Cosmochim Acta 60(2):337–347. https://doi.org/10.1016/0016-7037(95)00395-9

Benetti M, Reverdin G, Pierre C, Merlivat L, Risi C, Steen-Larsen HC, Vimeux F (2014) Deuterium excess in marine water vapor: dependency on relative humidity and surface wind speed during evaporation. J Geophys Res Atmos 119(2):584–593. https://doi.org/10.1002/2013jd020535

Bodhankar N, Chatterjee B (1994) Pollution of limestone aquifer due to urban waste–disposal around Raipur, Madhya-Pradesh, India. Environ Geol 23(3):209–213. https://doi.org/10.1007/bf00771790

Carlson PE, Miller NR, Banner JL, Breecker DO, Casteel RC (2018) The potential of near-entrance stalagmites as high-resolution terrestrial paleoclimate proxies: application of isotope and trace-element geochemistry to seasonally-resolved chronology. Geochim Cosmochim Acta 235:55–75. https://doi.org/10.1016/j.gca.2018.04.036

Carroll S, Goonetilleke A (2005) Assessment of high density of onsite wastewater treatment systems on a shallow groundwater coastal aquifer using PCA. Environmetrics 16(3):257–274. https://doi.org/10.1002/Env.698

Chen C, Li T (2018) Geochemical characteristics of cave drip water respond to ENSO based on a 6–year monitoring work in Yangkou Cave, Southwest China. J Hydrol 516:896–907. https://doi.org/10.1016/j.jhydrol.2018.04.061

Craig H (1961) Isotopic variations in meteoric waters. Science 133(3465):1702–1703. https://doi.org/10.1126/science.133.3465.1702

Dansgaard W (1964) Stable isotopes in precipitation. Tellus 16(4):436–468. https://doi.org/10.1111/j.2153-3490.1964.tb00181.x10.1111/j.2153-3490.1964.tb00181.x

Dodgen LK, Kelly WR, Panno SV, Taylor SJ, Armstrong DL, Wiles KN, Zhang Y, Zheng W (2017) Characterizing pharmaceutical, personal care product, and hormone contamination in a karst aquifer of southwestern Illinois, USA, using water quality and stream flow parameters. Sci Total Environ 578:281–289. https://doi.org/10.1016/j.scitotenv.2016.10.103

Duque C, López-Chicano M, Calvache ML, Martín-Rosales W, Gómez-Fontalva JM, Crespo F (2011) Recharge sources and hydrogeological effects of irrigation and an influent river identified by stable isotopes in the Motril-Salobrena aquifer (southern Spain). Hydrol Process 25(14):2261–2274. https://doi.org/10.1002/hyp.799010.1002/hyp.7990

Ekmekci M (2005) Pesticide and nutrient contamination in the Kestel Polje-Kirkgoz karst springs, southern Turkey. Environ Geol 49(1):19–29. https://doi.org/10.1007/s00254-005-0022-2

Field MS, Leij FJ (2012) Solute transport in solution conduits exhibiting multi-peaked breakthrough curves. J Hydrol 440–441:26–35. https://doi.org/10.1016/j.jhydrol.2012.03.018

Florea LJ, McGee DK (2010) Stable isotopic and geochemical variability within shallow groundwater beneath a hardwood hammock and surface water in an adjoining slough (Everglades National Park, Florida, USA). Isot Environ Health Stud 46(3):190–209. https://doi.org/10.1080/10256016.2010.494770

Ford DC, Williams PW (2007) Karst hydrogeology and geomorphology, Wiley, Chichester, UK

Gat J (2010) Isotope hydrology: a study of the water cycle. Imperial College Press, London

General Administration of Quality Supervision, Inspection and Quarantine of the People's Republic of China (2017) Standard for groundwater quality (GB/T 14848–2017) (in Chinese without English abstract). General Administration of Quality Supervision, Inspection and Quarantine, Beijing, China

Geyer T, Birk S, Licha T, Liedl R, Sauter M (2007) Multitracer test approach to characterize reactive transport in karst aquifers. Ground Water 45(1):36–45. https://doi.org/10.1111/j.1745-6584.2006.00261.x

Ghobadi MH, Taheri M, Taheri K (2017) Municipal solid waste landfill siting by using analytical hierarchy process (AHP) and a proposed karst vulnerability index in Ravansar County, west of Iran. Environ Earth Sci 76:78. https://doi.org/10.1007/s12665-017-6392-4

Goldscheider N (2005) Karst groundwater vulnerability mapping: application of a new method in the Swabian Alb, Germany. Hydrogeol J 13:555–564. https://doi.org/10.1007/s10040-003-0291-3

Goldscheider N (2008) A new quantitative interpretation of the long-tail and plateau-like breakthrough curves from tracer tests in the artesian karst aquifer of Stuttgart, Germany. Hydrogeol J 16:1311–1317. https://doi.org/10.1007/s10040-008-0307-0

Goldscheider N, Hötzl H, Käss W, Ufrecht W (2003) Combined tracer tests in the karst aquifer of the artesian mineral springs of Stuttgart, Germany. Environ Geol 43(8):922–929. https://doi.org/10.1007/s00254-002-0714-9

Goldscheider N, Meiman J, Pronk M, Smart C (2008) Tracer tests in karst hydrogeology and speleology. Int J Speleol 37(1):27–40. https://doi.org/10.5038/1827-806X.37.1.3

Gonfiantini R, Roche M, Olivry J, Fontes J, Zuppi GM (2001) The altitude effect on the isotopic composition of tropical rains. Chem Geol 181(1–4):147–167. https://doi.org/10.1016/S0009-2541(01)00279-0

Gong X, Chen Z, Luo Z (2014) Spatial distribution, temporal variation, and sources of heavy metal pollution in groundwater of a century-old nonferrous metal mining and smelting area in China. Environ Monit Assess 186(12):9101–9116. https://doi.org/10.1007/s10661-014-4069-y

Grimmeisen F, Lehmann MF, Liesch T, Goeppert N, Klinger J, Zopfi J, Goldscheider N (2017) Isotopic constraints on water source mixing, network leakage and contamination in an urban groundwater system. Sci Total Environ 583:202–213. https://doi.org/10.1016/j.scitotenv.2017.01.054

Guo X, Jiang G, Gong X, Yin J, Wu X (2015) Recharge processes on typical karst slopes implied by isotopic and hydrochemical indexes in Xiaoyan Cave, Guilin, China. J Hydrol 530:612–622. https://doi.org/10.1016/j.jhydrol.2015.09.065

Huang T, Pang Z (2012) The role of deuterium excess in determining the water salinisation mechanism: a case study of the arid Tarim River basin, NW China. Appl Geochem 27(12):2382–2388. https://doi.org/10.1016/j.apgeochem.2012.08.015

Huth AK, Leydecker A, Sickman JO, Bales RC (2004) A two-component hydrograph separation for three high-elevation catchments in the Sierra Nevada, California. Hydrol Process 18(9):1721–1733. https://doi.org/10.1002/Hyp.1414

Iverson G, O'Driscoll MA, Humphrey CP, Manda AK, Anderson-Evans E (2015) Wastewater nitrogen contributions to coastal plain watersheds, NC, USA. Water Air Soil Pollut 226(10):325. https://doi.org/10.1007/S11270-015-2574-4

Jiang Y, Zhang C, Yuan D, Zhang G, He R (2008) Impact of land use change on groundwater quality in a typical karst watershed of Southwest China: a case study of the Xiaojiang watershed, Yunnan Province. Hydrogeol J 16(4):727–735. https://doi.org/10.1007/s10040-007-0259-9

Jiang Y, Wu Y, Yuan D (2009) Human impacts on karst groundwater contamination deduced by coupled nitrogen with strontium isotopes in the Nandong Underground River system in Yunan, China. Environ Sci Technol 43(20):7676–7683. https://doi.org/10.1021/es901602t

Jiang Y, Hu Y, Schirmer M (2013) Biogeochemical controls on daily cycling of hydrochemistry and $\delta^{13}C$ of dissolved inorganic carbon in a karst spring-fed pool. J Hydrol 478:157–168. https://doi.org/10.1016/j.jhydrol.2012.12.001

Jin L, Siegel DI, Lautz LK, Lu Z (2012) Identifying streamflow sources during spring snowmelt using water chemistry and isotopic composition in semi-arid mountain streams. J Hydrol 470–471:289–301. https://doi.org/10.1016/j.jhydrol.2012.09.009

Katz BG, Griffin DW, McMahon PB, Harden HS, Wade E, Hicks R, Chanton JP (2010) Fate of effluent-borne contaminants beneath septic tank drainfields overlying a karst aquifer. J Environ Qual 39:1181–1195. https://doi.org/10.2134/Jeq2009.0244

Klaus J, McDonnell JJ (2013) Hydrograph separation using stable isotopes: review and evaluation. J Hydrol 505:47–64. https://doi.org/10.1016/j.jhydrol.2013.09.006

Kogovšek J, Petrič M (2013) Increase of vulnerability of karst aquifers due to leakage from landfills. Environ Earth Sci 70(2):901–912. https://doi.org/10.1007/s12665-012-2180-3

Larssen T, Carmichael GR (2000) Acid rain and acidification in China: the importance of base cation deposition. Environ Pollut 110(1):89–102. https://doi.org/10.1016/S0269-7491(99)00279-1

Larssen T, Lydersen E, Tang D, He Y, Gao J, Liu H, Duan L, Seip HM, Vogt RD, Mulder J, Shao M, Wang Y, Shang H, Zhang X, Solberg S, Aas W, Okland T, Eilertsen O, Angell V, Li Q, Zhao D, Xiang R, Xiao J, Luo J (2006) Acid rain in China. Environ Sci Technol 40(2):418–425. https://doi.org/10.1021/Es0626133

Lauber U, Goldscheider N (2014) Use of artificial and natural tracers to assess groundwater transit–time distribution and flow systems in a high-alpine karst system (Wetterstein Mountains, Germany). Hydrogeol J 22(8):1807–1824. https://doi.org/10.1007/s10040-014-1173-6

Laudon H, Hemond HF, Krouse R, Bishop KH (2002) Oxygen 18 fractionation during snowmelt: implications for spring flood hydrograph separation. Water Resour Res 38(11):40–41–41–10. https://doi.org/10.1029/2002wr001510

Lettingue M (2007) Vulnerability and risk mapping, tracer tests and microbiological monitoring to assess the human impact on an UNESCO world heritage candidate site, the Jinfo karst plateau, China. MSc Thesis, Université de Neuchâtel, Neuchâtel, France

Magal E, Arbel Y, Caspi S, Glazman H, Greenbaum N, Yechieli Y (2013) Determination of pollution and recovery time of karst springs, an example from a carbonate aquifer in Israel. J Contam Hydrol 145:26–36. https://doi.org/10.1016/j.jconhyd.2012.10.010

Mahler B, Massei N (2007) Anthropogenic contaminants as tracers in an urbanizing karst aquifer. J Contam Hydrol 91(1–2):81–106. https://doi.org/10.1016/j.jconhyd.2006.08.010

Maurya AS, Shah M, Deshpande RD, Bhardwaj RM, Prasad A, Gupta SK (2011) Hydrograph separation and precipitation source identification using stable water isotopes and conductivity: River Ganga at Himalayan foothills. Hydrol Process 25(10):1521–1530. https://doi.org/10.1002/Hyp.7912

Mellander PE, Jordan P, Wall DP, Melland AR, Meehan R, Kelly C, Shortle G (2012) Delivery and impact bypass in a karst aquifer with high phosphorus source and pathway potential. Water Res 46(7):2225–2236. https://doi.org/10.1016/j.watres.2012.01.048

Milenic D, Milankovic D, Petric M, Savic N, Vranjes A (2014) Integrated management of karstic waters: a case study of the Zlatibor Mountain Massif, Serbia. Global NEST J 16(4):717–731

Mook WG (2000) Environmental isotopes in the hydrological cycle: principles and applications. UNESCO, Paris

Pape JR, Banner JL, Mack LE, Musgrove M, Guilfoyle A (2010) Controls on oxygen isotope variability in precipitation and cave drip waters, central Texas, USA. J Hydrol 385(1–4):203–215. https://doi.org/10.1016/j.jhydrol.2010.02.021

Pei YS, Luan ZK, Barber C, Williamson D (2003) Assessment of the environmental impact of artificial effluent lagoon in Jiayuguan City of China. J Environ Sci-China 15(4):525–530. https://doi.org/10.1001/0742(2003)04-0525-06

Pronk M, Goldscheider N, Zopfi J (2007) Particle–size distribution as indicator for fecal bacteria contamination of drinking water from karst springs. Environ Sci Technol 41(24):8400–8405. https://doi.org/10.1021/es071976f

Rapti-Caputo D, Martinelli G (2009) The geochemical and isotopic composition of aquifer systems in the deltaic region of the Po River plain (northern Italy). Hydrogeol J 17(2):467–480. https://doi.org/10.1007/s10040-008-0370-6

Schiavo MA, Hauser S, Povinec PP (2009) Stable isotopes of water as a tool to study groundwater–seawater interactions in coastal southeastern Sicily. J Hydrol 364(1–2):40–49. https://doi.org/10.1016/j.jhydrol.2008.10.005

Schmidt S, Geyer T, Marei A, Guttman J, Sauter M (2013) Quantification of long-term wastewater impacts on karst groundwater resources in a semi-arid environment by chloride mass balance methods. J Hydrol 502:177–190. https://doi.org/10.1016/j.jhydrol.2013.08.009

Schnegg PA, Costa R (2002) Tracer tests made easier with field fluorometers. Bull Hydrogeol 20(5):89–91

State Bureau of Technical Supervision of China (2008) Method for examination of drinking natural mineral water (GB/T8538–2008) (in Chinese without English abstract). State Bureau of Technical Supervision of China, Beijing

Tang D, Lydersen E, Seip HM, Angell V, Eilertsen O, Larssen T, Liu X, Kong G, Mulder J, Semb A, Solberg S, Torseth K, Vogt RD, Xiao J, Zhao D (2001) Integrated monitoring program on acidification of Chinese terrestrial systems (impacts): a Chinese-Norwegian cooperation project. Water Air Soil Poll 130(1–4):1073–1078. https://doi.org/10.1023/A:1013982300245

Toor, GS, Toor M, Obrez T (2011) Onsite sewage treatment and disposal systems: an overview, Institute of Food and Agric Sci, University of Florida, Gainesville, FL. http://edis.ifas.ufl.edu/ss549. Accessed July 23 2018

Turner KW, Edwards TWD, Wolfe BB (2014) Short communication characterising runoff generation processes in a lake-rich thermokarst landscape (Old Crow Flats, Yukon, Canada) using $\delta^{18}O$, $\delta^{2}H$ and d-excess measurements. Permafrost Periglac 25(1):53–59. https://doi.org/10.1002/ppp.1802

Umezawa Y, Hosono T, Onodera S, Siringan F, Buapeng S, Delinom R, Yoshimizu C, Tayasu I, Nagata T, Taniguchi M (2009) Erratum to "Sources of nitrate and ammonium contamination in groundwater under developing Asian megacities". Sci Total Environ 407(9): 3219–3231. https://doi.org/10.1016/j.scitotenv.2009.01.047

UNESCO (2014a) Decision: 38 COM 8B.9, South China Karst (China) (extension). http://whc.unesco.org/en/decisions/6094. Accessed July 23, 2018

UNESCO (2014b) WHC-14/38.COM/16: report of the decisions adopted by the World Heritage Committee at its 38th session (Doha, 2014). http://whc.unesco.org/en/documents/131277/,%20WHC-14/38.COM/16. Accessed July 23, 2018

USEPA (2002) Onsite wastewater treatment systems manual (EPA/625/R-00/008). Office of Water, Office of Research and Development, USEPA, Washington, DC

Vanderzalm JL, Jeuken BM, Wischusen JDH, Pavelic P, Le Gal La Salle C, Knapton A, Dillon PJ (2011) Recharge sources and hydrogeochemical evolution of groundwater in alluvial basins in arid central Australia. J Hydrol 397(1–2):71–82. https://doi.org/10.1016/j.jhydrol.2010.11.035

Wang H, Li T, Yuan N, Li J (2014) Environmental signification and characteristics of δD and $\delta^{18}O$ variation in drip water in Yangkou Cave, Chongqing China (in Chinese without English abstract). Carsolog Sin 33:146–155

Wang S (2011) The new method of engineering geology (in Chinese without English abstract). Yinshengyingxiang Press, China

Wu Y, Jiang Y, Yuan D, Li L (2008) Modeling hydrological responses of karst spring to storm events: example of the Shuifang spring (Jinfo Mt., Chongqing, China). Environ Geol 55(7):1545–1553. https://doi.org/10.1007/s00254-007-1105z

Xiao K (2015) Analysis of hydrogeochemistry and hydrogen and oxygen isotopes of surface surface water and groundwater in Jinfo Mt (in Chinese with English abstract). MSc Thesis, Southwest University, Chongqing, China

Yang M, Hens L, Ou X, De Wulf R (2009) Tourism: an alternative to development? Mt Res Dev 29(1):75–81. https://doi.org/10.1659/Mrd.1051

Yang P, Yuan D, Yuan W, Kuang Y, Jia P, He Q (2010) Formations of groundwater hydrogeochemistry in a karst system during storm events as revealed by PCA. Chin Sci Bull 55(14):1412–1422. https://doi.org/10.1007/s11434-010-0083-9

Yang P, Yuan D, Ye X, Xie S, Chen X, Liu Z (2013) Sources and migration path of chemical compositions in a karst groundwater system during rainfall events. Chin Sci Bull 58(20):2488–2496. https://doi.org/10.1007/s11434-013-5762-x

Zang H, Zheng X, Qin Z, Jia Z (2015) A study of the characteristics of karst groundwater circulation based on multi-isotope approach in the Liulin spring area, North China. Isot Environ Health Stud 51(2):271–284. https://doi.org/10.1080/10256016.2015.987275

Zhu Y, Ye M, Roeder E, Hicks RW, Shi L, Yang J (2016) Estimating ammonium and nitrate load from septic systems to surface water bodies within ArcGIS environments. J Hydrol 532:177–192. https://doi.org/10.1016/j.jhydrol.2015.11.017